

SCIENTIFIC REPORTS

OPEN

Nanoscale enhancement of photoconductivity by localized charge traps in the grain structures of monolayer MoS₂

Myungjae Yang, Tae-Young Kim, Takhee Lee & Seunghun Hong

We report a method for mapping the nanoscale anomalous enhancement of photoconductivity by localized charge traps in the grain structures of a molybdenum disulfide (MoS₂) monolayer. In this work, a monolayer MoS₂ film was laterally scanned by a nanoscale conducting probe that was used to make direct contact with the MoS₂ surface. Electrical currents and noise maps were measured through the probe. By analyzing the data, we obtained maps for the sheet resistance and charge trap density for the MoS₂ grain structures. The maps clearly show grains for which sheet resistance and charge trap density were lower than those of the grain boundaries. Interestingly, we found an unusual inverse proportionality between the sheet resistance and charge trap density in the grains, which originated from the unique role of sulfur vacancies acting as both charge hopping sites and traps in monolayer MoS₂. In addition, under light illumination, the larger the trap density of a region was, the larger the photocurrent of the region was, indicating anomalous enhancement of the photocurrent by traps. Since our method provides valuable insights to understand the nanoscale effects of traps on photoconductive charge transport, it can be a powerful tool for noise studies and the practical application of two-dimensional materials.

Atomically layered transition metal dichalcogenides (TMDCs) have emerged as promising two-dimensional materials for future applications^{1,2}. Since TMDCs have unique properties, including an intrinsic band gap varying with the number of layers, a direct band gap and strong spin-orbit coupling in monolayers²⁻⁴, they have been widely studied¹⁻⁷. As a typical TMDC material, molybdenum disulfide (MoS₂) has a layered structure with a monolayer thickness of ~0.7 nm¹. The layers of MoS₂ are held together by weak van der Waals interactions^{1,4}. Due to the direct band gap of ~1.8 eV in the monolayer², MoS₂ has great potential for device applications, especially in optoelectronics such as photodetectors⁵, light-emitting diodes⁶ and solar cells⁷. However, the nanoscale characteristics of electrical conduction and photoconduction in the grain structure of a MoS₂ layer are not fully understood.

In many applications, electrical noise is an important factor, which significantly affects the performance of devices⁸. In addition, noise data often provide critical information for understanding the internal structures and defects of electronic materials such as MoS₂, and thus, methods for the measurement of the noise source activities in electronic materials would be very useful tools for engineering high performance devices for optoelectronic⁹ and electrochemical applications¹⁰. Until now, noise studies for specific materials have usually been carried out using noise measurements on devices based on the materials. For example, the characteristics and origins of electrical noise in MoS₂ devices were revealed by measuring the gating effect on electrical noise in MoS₂-based electrical channels¹¹⁻¹⁴. Meanwhile, a method using a conducting atomic force microscopy (AFM) enabled the direct imaging of localized noise sources such as charge traps in materials¹⁵⁻¹⁷. A previous study utilized this noise microscopy method to obtain a map of the charge traps on a graphene sample¹⁵. However, noise microscopy analysis of two-dimensional charge transport in a photoconductive channel has not been reported before.

Herein, we report the observation of the nanoscale anomalous enhancement of photoconductivity induced by localized charge traps in the grain structures of monolayer MoS₂. In this work, a nanoscale conducting probe was used to make direct contact on a monolayer MoS₂ sample on a SiO₂ substrate, and, then, scanned laterally

Department of Physics and Astronomy, and Institute of Applied Physics, Seoul National University, Seoul, 08826, Korea. Correspondence and requests for materials should be addressed to S.H. (email: seunghun@snu.ac.kr)

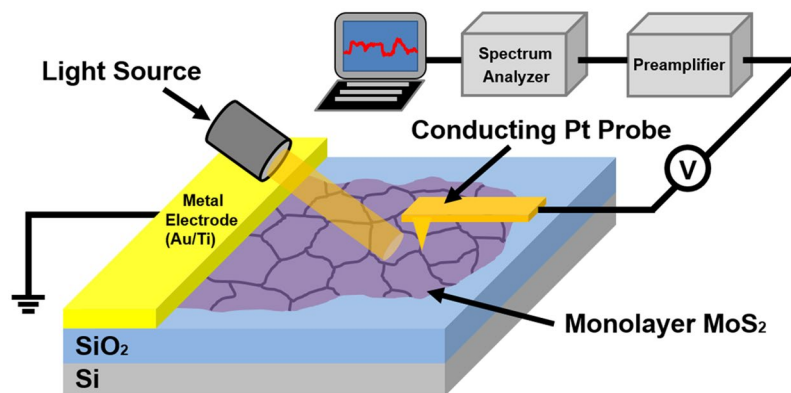


Figure 1. Schematic diagram depicting the scanning noise measurement setup for a MoS₂ monolayer sample grown onto a SiO₂/Si substrate. A conducting AFM probe laterally scanned the MoS₂ surface under ambient conditions, while making direct contact with the sample. Electrical current and noise PSD maps were simultaneously measured through the probe. The measured data were analyzed to obtain maps of the sheet resistance and charge trap density distributions in MoS₂ grain structures.

while mapping the electrical currents and noise through the probe. Then, the measured current and noise maps were analyzed to obtain maps for the sheet resistance and localized charge trap distributions in the MoS₂ grain structures. The maps clearly show multiple MoS₂ grains with rather low sheet resistances and charge trap densities compared with their boundaries. Interestingly, unlike other common conducting channels, the sheet resistance inside the grains was found to be inversely proportional to the charge trap density, which was attributed to the unique role of sulfur vacancies working as both charge hopping sites and charge traps in MoS₂. Furthermore, under light illumination, regions with larger charge trap densities exhibited larger photocurrents, indicating that photocurrents were enhanced by charge trap sites. This method provides a valuable insight for the nanoscale effects of charge traps on the photoconductive charge transport, and, thus, can be utilized for various electrical noise research and practical device applications based on two-dimensional materials.

Results and Discussion

Experimental setup. Figure 1 shows the schematic diagram of our current and noise measurement setup. A MoS₂ monolayer film was grown onto a SiO₂/Si substrate by a chemical vapor deposition (CVD) method. For the noise microscopy measurement, a Pt-based conducting probe (25Pt300B, Park Systems) installed in an AFM (XE-70, Park Systems) was used to make a direct contact with the surface of the MoS₂ film under ambient conditions. Then, a direct current (DC) bias voltage of 5 V was applied to the Pt probe using a DC power supply (DS345, Stanford Research Systems). The current through the Pt probe was measured and converted to amplified voltage signals by a low-noise preamplifier (SR570, Stanford Research Systems). Simultaneously, electrical noise (the fluctuating component of a current signal) was collected using a band-pass filter (6 dB) in the SR570 preamplifier. We utilized a homemade root mean square (RMS)-to-DC converter to obtain the RMS power of the noise. The absolute noise power spectral density (PSD) at the central frequency of the band-pass filter was obtained by dividing the square of the measured RMS noise power with the bandwidth of the band-pass filter. Using this setup, two-dimensional maps for the topography, current and noise PSD were obtained at the same time by scanning the AFM probe on the MoS₂ sample. The mapping data were analyzed to obtain maps of the sheet resistance and charge trap density. In addition, we measured changes in the current and noise maps by white light illumination using a light source (LS-F100HS).

Characterization of CVD-grown monolayer MoS₂. Figure 2(a) shows the optical microscopy image of a MoS₂ film. The MoS₂ was synthesized via CVD on a SiO₂/Si substrate. The MoS₂ film exhibited a darker purple color than the SiO₂ region. The constant color contrast of the MoS₂ region implies that the thickness of the MoS₂ film was rather uniform¹⁸. The image indicates that the surface of the MoS₂ sample was uniform and clean.

The layer number of the MoS₂ film was characterized by Raman spectroscopy (Fig. 2(b)). We used a Raman microscope (XperRam 200, Nanobase) with a 532 nm laser. The Raman spectrum of our MoS₂ film shows two major peaks at 383.4 and 403.7 cm⁻¹. The interval for the peaks is approximately 20.3 cm⁻¹. These two peaks correspond to the E_{2g}¹ (383.4 cm⁻¹) and A_{1g} (403.7 cm⁻¹) modes of MoS₂¹⁸. It is known that the interval for the two major peaks decreases as the number of layers in MoS₂ decreases, being ~20 cm⁻¹ in the case of a monolayer¹⁹. Hence, the Raman spectrum indicates that the MoS₂ film consisted of a single atomic layer. The topography image of the MoS₂ film obtained by AFM measurement also supported the observation of monolayer formation in our film (Fig. S1 in the Supplementary Information).

Figure 2(c) shows the current-voltage (*I-V*) characteristics of our MoS₂ sample. A bias voltage was applied to the Pt probe and swept from -5 to 5 V. The *I-V* graph exhibits asymmetric and nonlinear behavior. The nonlinear curve implies that Schottky contacts are formed between the MoS₂ layer and the electrode, presumably due to the large band gap of MoS₂²⁰. Since the work function of the Pt probe is larger than that of the Au/Ti electrode, a negative bias on the Pt probe would worsen the Schottky barrier between the MoS₂ film and the Au/Ti electrode, resulting in a low current level. This result shows the Schottky barrier at the MoS₂-metal contacts may have a

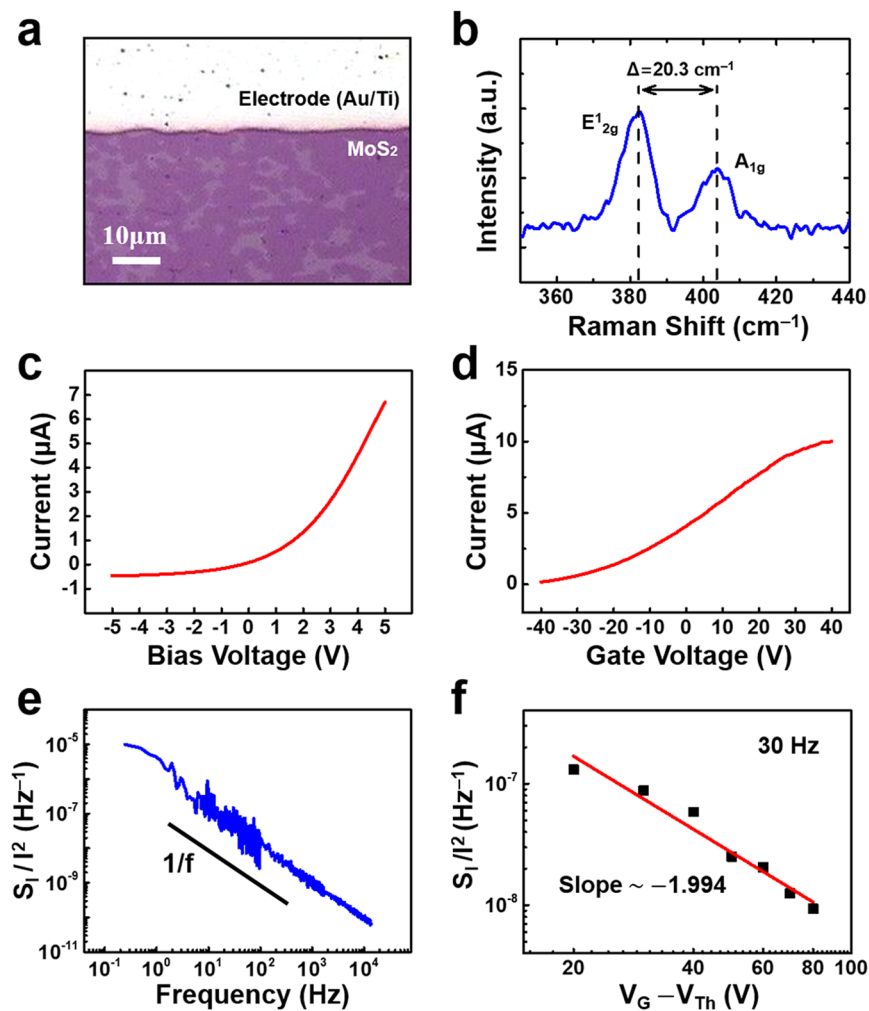


Figure 2. Characterization of a monolayer MoS₂ sample. **(a)** Optical image of monolayer MoS₂ grown onto a SiO₂/Si substrate. The constant color contrast indicates the uniform thickness of the MoS₂ film. **(b)** Raman spectroscopy data for the sample. Two major peaks at 383.4 and 403.7 cm⁻¹ correspond to the E_{12g} and A_{1g} modes of MoS₂, respectively. The interval of 20.3 cm⁻¹ between the two peaks indicates the monolayer of MoS₂. **(c)** Current-voltage (*I*-*V*) curve measured on the sample. **(d)** Current measured by sweeping a gate voltage (*V*_G). The threshold voltage (*V*_{Th}) was estimated to be ~-40 V. **(e)** Current-normalized noise PSD (*S*_I/*I*²) dependence on frequency. A 1/*f* noise behavior was observed. **(f)** *S*_I/*I*² at 30 Hz as a function of *V*_G. The slope of the fitted line is -1.994, which is close to the value of -2 expected for carrier number fluctuations as the dominant origin for the noise generation.

significant effect on the *I*-*V* characteristics, as reported previously²¹. Figure 2(d) shows a back gate effect on the sample at a source-drain bias voltage of 3 V. The gate voltage (*V*_G) was swept from -40 to 40 V using the SiO₂ substrate as a back gate. The result shows an increasing current as the gate voltage was swept from negative to positive values, indicating typical *n*-type behavior for the MoS₂ channel¹¹⁻¹⁴. The threshold voltage (*V*_{Th}) (the minimum gate voltage required to form a conducting channel) was obtained from the curve. The threshold voltage (*V*_{Th}) was estimated to be ~-40 V, which is the *V*_G-axis intercept of the extrapolated line for the maximum slope region in the curve. The electrical properties of the MoS₂ sample were comparable to those found in a previous study¹⁸, confirming the uniform quality of our MoS₂ film.

In Fig. 2(e), the frequency dependence of the current-normalized noise PSD (*S*_I/*I*²) is plotted on a log scale. A spectrum analyzer (SR780, Stanford Research Systems) was utilized to measure the noise spectrum. The *S*_I/*I*² exhibited a 1/*f* noise behavior, as reported in previous noise studies on MoS₂ devices¹¹⁻¹⁴. In our previous work, we showed that noise PSDs exhibited 1/*f*² (or Lorentzian) noise behavior when a current noise was generated by a few trap states that had rather uniform trapping times^{15,17}. However, noise spectra exhibited 1/*f* behavior¹⁵⁻¹⁷ when there were many trap states with various trapping times. The 1/*f* noise behavior in our plot implies that the noise was generated by many different noise sources such as charge traps in the MoS₂ sample.

Previously, a 1/*f* noise was suggested to originate from *mobility fluctuations* or *carrier number fluctuations* and that in each case *S*_I/*I*² is differently related to carrier density^{10,11,22,23}. To clarify a dominant origin, we measured *S*_I/*I*² at different gate voltages (*V*_G) since the carrier density can be modulated by *V*_G. Fig. 2(f) shows a plot of *S*_I/*I*²

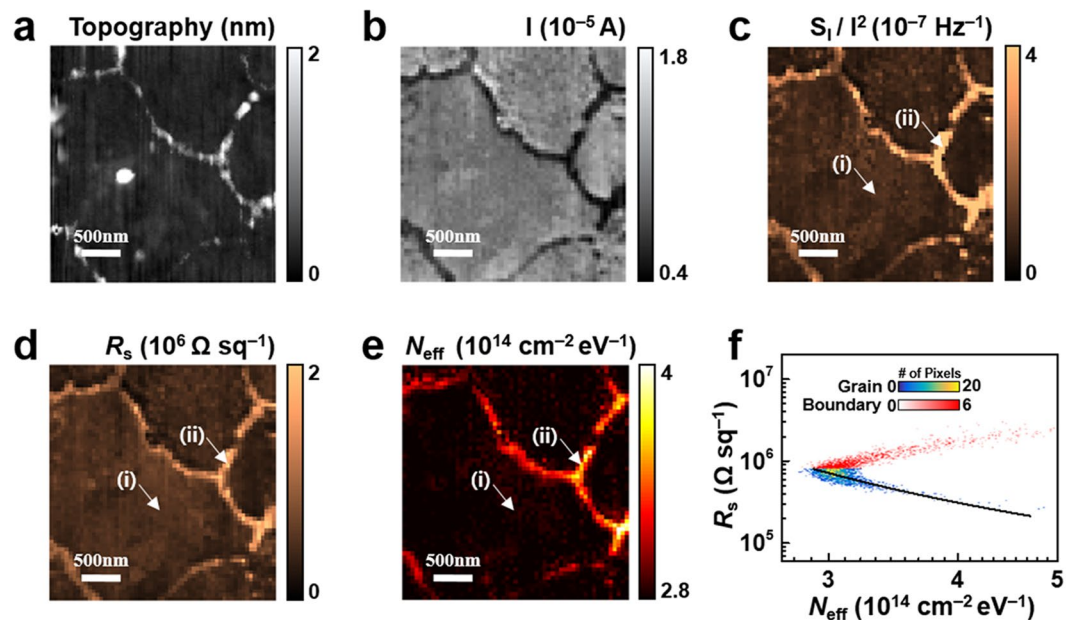


Figure 3. Mapping of sheet resistance and charge trap density in the grain structure of a MoS₂ monolayer. (a) AFM topography image of the MoS₂ monolayer film. (b) Current (I) map of the MoS₂ film. A bias voltage of 5 V was applied to the film through a metal electrode. The data show clear separation between grains and boundaries. (c) Current-normalized noise PSD (S_I/I^2) map (at 17.3 Hz) for the film. The large S_I/I^2 values in the boundaries indicate that the existence of dense defects act as noise sources. (d) Sheet resistance (R_s) map for the MoS₂ sample. The boundary showed larger R_s than the grain due to structural disorder. (e) Charge trap density (N_{eff}) map for the sample. The boundary regions showed higher N_{eff} than the grain regions. (f) Scatter plot showing the relation between N_{eff} and R_s . A negative correlation between N_{eff} and R_s was observed in the grains, while the boundaries showed a positive correlation.

values over V_G . The S_I/I^2 was measured while a V_G ranging from -20 to 40 V was applied to the SiO₂ back gate. The slope of the fitted line in the log-log plot is estimated to be -1.994 , which is close to -2 , as expected for *carrier number fluctuations*^{14,22,23}. This implies that *carrier number fluctuations* were the dominant mechanism for noise generation in our MoS₂ sample, as reported previously^{12,14}.

Charge trap distribution in the grain structure of monolayer MoS₂. Figure 3(a) shows the AFM topography image of a MoS₂ monolayer. The surface area ($3 \times 3 \mu\text{m}^2$) was scanned by an AFM probe. In the image, dark regions (film thickness < 1 nm) are distinguished from bright regions (film thickness ~ 2 nm). Additionally, there is a bright dot near the center of the grain. From the reported thickness of a MoS₂ monolayer (~ 0.7 nm)¹, we can consider the dark area as grains of MoS₂ and the bright area as grain boundaries. The dot near the center of the grain would be a precursor for the CVD process of a MoS₂ film, as reported previously²⁴. The difference in thickness between grain and boundary regions can be explained via a boundary formation mechanism. Typically, the growth of individual grains is known to stop when chemical bonds are formed between the grains²⁵. However, it is common that the neighboring grains proceed to grow even after they encounter each other, forming additional layers. Thus, layer-overlapping without chemical bonds can occur, resulting in thicker boundaries²⁵. The topography image indicates the cleanliness of the film, which showed no wrinkles or severely rough surface regions.

Figure 3(b) shows a current map for the MoS₂ sample. The current was measured through the conducting probe while a DC bias voltage of 5 V was applied to the Au/Ti electrode. During the measurement, the sample was held under dark conditions to exclude photocurrents. In the map, bright and dark regions are clearly distinguished. The dark regions ($\sim 10^{-6}$ A), which correspond to boundary regions, showed lower currents compared to the grain regions ($\sim 10^{-5}$ A). This current difference could arise from structural disorder in the boundaries, which obstructs current flow. In a grain boundary region, the atomic structure could be different with that inside the grain due to the different orientation of adjacent grains, or grain overlapping and ruptures. Previous works show that various defects in boundaries, such as line dislocations and complex atomic ring structures, induce mid-gap states and decrease the band gap^{26–29}. In addition, grain overlapping and ruptures could generate grain edges with unsaturated bonds, which lead to the intrinsic modification of the electronic structure due to the loss of periodicity²⁸. The result shows success mapping of localized currents via a stable contact between the probe and the MoS₂ film, which is important for reliable electrical measurements.

Figure 3(c) shows a S_I/I^2 map (at 17.3 Hz) obtained from a noise PSD map measured simultaneously with the current map (Fig. 3(b)). Here, the noise PSD map (S_I) at 17.3 Hz was divided by the square of the current (I) map. The S_I/I^2 values were $\sim 1.12 \times 10^{-7} \text{ Hz}^{-1}$ inside a grain (arrowed by (i)) and $\sim 3.96 \times 10^{-7} \text{ Hz}^{-1}$ inside a boundary (arrowed by (ii)), indicating a higher noise level in the boundary than in the grain. The high S_I/I^2 in the boundary

implies that a large electrical noise was generated in the grain boundaries. Previously, it was reported that defects and disorders in a MoS₂ layer induce localized states within a band gap³⁰, which can act as traps^{31,32} and generate current noise by trapping and detrapping charge carriers. Hence, the large electrical noise from boundaries can be attributed to rather high density of defects in the area. It is remarkable that noise contributions from each localized area for the monolayer MoS₂ could be distinguished in our result, providing important information about how noise levels differ in grain structures.

Figure 3(d) shows a sheet resistance (R_s) map of the monolayer MoS₂ film. To obtain the R_s distribution, we performed computer calculations based on an iterative method developed in our previous work¹⁵. In brief, we calculated the R_s map, which reproduced the measured current map in Fig. 3(b), via an iterative method. In the map, grains and their boundaries exhibit a clear difference in R_s . The R_s values were $\sim 8.28 \times 10^5 \Omega \text{ sq}^{-1}$ inside a grain (arrowed by (i)) and $\sim 2.05 \times 10^6 \Omega \text{ sq}^{-1}$ inside a boundary (arrowed by (ii)), showing ~ 2.5 times higher values in boundaries than in grains. The result was consistent with the reported R_s values for CVD-grown monolayer MoS₂ (10^5 – $10^6 \Omega \text{ sq}^{-1}$)^{6,26,33}. The large R_s of the boundary regions could originate from numerous scattering centers due to structural disorder^{25,34}. Additionally, the R_s difference between grains and boundaries was similar to that measured for intra- and inter-grain channels in field effect transistors (FETs) in a previous study²⁶. However, it should be mentioned that previous measurements had difficulty in clearly distinguishing the localized resistance values for the grains and boundaries since the FET channels included both regions.

From the data in Fig. 2(f), we showed that the $1/f$ noise of our MoS₂ channel (Fig. 2(e)) was mainly generated by carrier number fluctuations. The number of carriers fluctuates since charge carriers are randomly trapped and detrapped by charge trap states, generating current noise³⁵. Using the differential method developed in our previous study¹⁵, an effective charge trap density (N_{eff}) (the integrated value of the charge trap density over the thickness) of a small area $\Delta x \Delta y$ at (x, y) on a sample surface is obtained as

$$N_{\text{eff}}(f, x, y) = \frac{(\Delta C)^2}{(I)^2} \frac{f}{kT} \times \frac{\Delta S_I(f, x, y)}{\Delta x \Delta y} \quad (1)$$

where ΔC , I , f , k , T and ΔS_I are the number of charge carriers, measured current, frequency, Boltzmann constant, temperature and noise PSD generated by the small area, respectively. In the case of $1/f$ noise, $\Delta S_I(f, x, y)$ is proportional to $1/f$. Then, $f \Delta S_I$ becomes f -independent, resulting in a f -independent $N_{\text{eff}}(f, x, y)$, i.e., $N_{\text{eff}}(x, y)$. To estimate ΔS_I , we considered a MoS₂ layer as a two-dimensional resistance network. This “network model” was shown to be a successful model in our previous study on graphene samples¹⁵. The ΔC in equation (1) was estimated from the charge carrier concentration. We calculated the charge carrier concentration (n) using $n = C_{\text{OX}}(V_G - V_{\text{Th}})/e$, where C_{OX} is the gate capacitance of the SiO₂ layer ($\sim 1.48 \times 10^{-8} \text{ F/cm}^2$), V_G is the gate voltage (0 V), V_{Th} is the threshold voltage ($\sim -40 \text{ V}$), and e is the elementary charge ($1.60 \times 10^{-19} \text{ C}$). The calculated value for n was $\sim 3.69 \times 10^{12} \text{ cm}^{-2}$. Then, ΔC could be calculated from $\Delta C = n \Delta x \Delta y$, where $\Delta x \Delta y$ is the effective contact area of the conducting Pt probe ($\sim 2000 \text{ nm}^2$). Eventually, we could estimate N_{eff} values at each point of the area scanned by a conducting AFM probe. Since N_{eff} is an integrated value over a thickness, it will be a useful value representing the effective density of charge traps in two-dimensional materials.

Figure 3(e) shows the effective charge trap density (N_{eff}) map of the MoS₂ monolayer. The map exhibits the areal density distribution of the charge traps on the sample. The N_{eff} value was $\sim 2.91 \times 10^{14} \text{ cm}^{-2} \text{ eV}^{-1}$ inside a grain (arrowed by (i)), while the boundary region (arrowed by (ii)) exhibited a N_{eff} value of $\sim 3.87 \times 10^{14} \text{ cm}^{-2} \text{ eV}^{-1}$, which was ~ 1.3 times higher in value than that of the grain. In a MoS₂ film, charge traps can be induced by defects including atomic vacancies, dangling bonds and impurities^{30–32}. Since defects in monolayer MoS₂ generate trap states within a band gap while defect-free monolayer MoS₂ shows no such states^{30,36}, N_{eff} corresponds to the density of traps generated by defects. The high N_{eff} in the boundary implies the existence of abundant charge traps, which originate from structural disorder of the boundaries^{25,34}. Charge traps in a MoS₂ sample can also be located in the underlying substrate. However, it should be noted that the N_{eff} values in our map were 2–3 orders of magnitude higher than the reported oxide trap density associated with SiO₂ substrates^{12,37}, indicating that the substrate was not the main origin for the generated noise. Instead, the N_{eff} could be attributed to defects generated during the CVD process under high temperature ($\sim 750 \text{ }^\circ\text{C}$) and low pressure ($\sim 10 \text{ Torr}$), as reported previously³⁸. Previously, it was reported that the presence of defects such as sulfur vacancies significantly affects the band structure of monolayer MoS₂ by introducing localized mid-gap states near the Fermi level, leading to a transition from a direct to indirect band gap³⁰. Our method provides a method to map localized density of charge traps in two-dimensional nanomaterials, which can be useful for studying charge traps in various other nanostructured materials.

Figure 3(f) shows a scatter plot for the relationship between N_{eff} and R_s for monolayer MoS₂ on a log-log scale. Each data point in the plot is obtained from the pixel area in the N_{eff} map (Fig. 3(e)) and the corresponding pixel area in the R_s map (Fig. 3(d)). The data points for the grains and boundaries were distinguished using the R_s map. The plot exhibits different tendencies for grain and boundary regions, showing a positive correlation in boundaries and a negative correlation in grains. The positive N_{eff} - R_s correlation in boundaries is similar to previously reported results on the relation between noise PSD and resistance in percolated systems^{38–41}. Since boundaries are highly disordered regions with many trap states, each pixel region in the boundaries can be considered as a localized percolation channel. In such a system, it was reported that both resistance and its fluctuation have a power law dependence on $(p - p_c)$, where p is the fraction of the conductive paths and p_c is the percolation threshold³⁹. Hence, the resistance of each pixel region (R_s , in our case) is related to its fluctuation as follows

$$\frac{\Delta S_R}{(R_s)^2} \propto (R_s)^w \quad (\text{at } p > p_c) \quad (2)$$

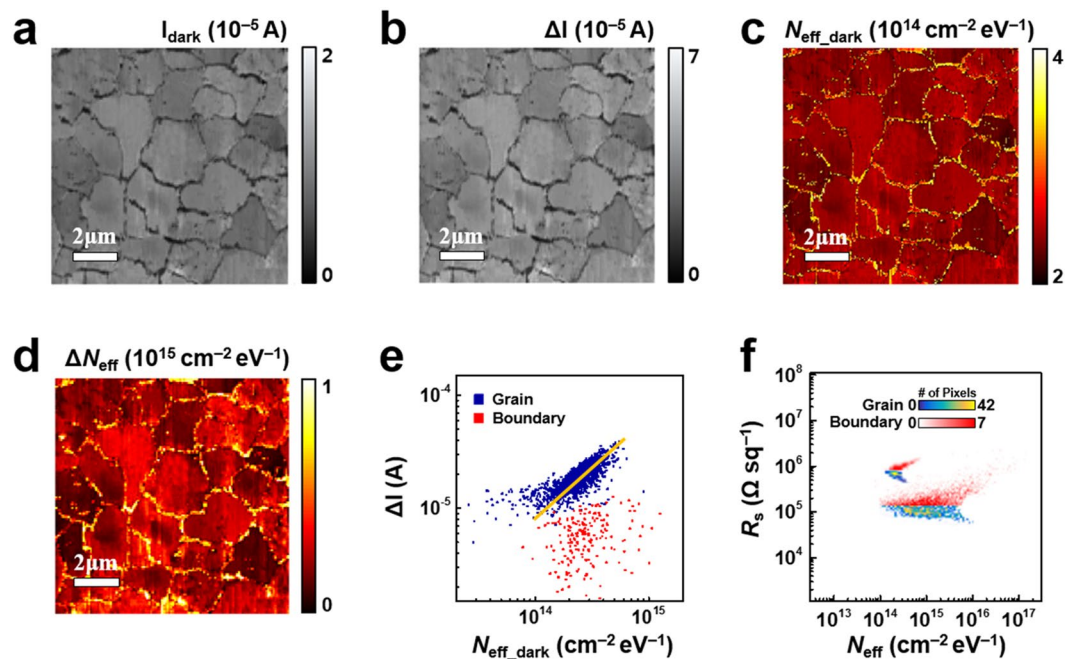


Figure 4. Changes in the current and charge trap density of a MoS₂ monolayer due to light illumination. (a) Current map measured under dark conditions. (b) Map of current change (ΔI) under illumination. Photocurrents were larger in grains than in boundaries. (c) Map of the charge trap density under the dark condition ($N_{\text{eff_dark}}$). (d) Map showing changes in charge trap density (ΔN_{eff}) due to illumination. The positive ΔN_{eff} arises from defect generation by absorbed photons. (e) Scatter plot exhibiting a correlation between $N_{\text{eff_dark}}$ and ΔI . The slope of the orange fitted line is ~ 0.9 , indicating linear proportionality. (f) Scatter plot of N_{eff} versus R_s under dark and illuminated conditions. The R_s generally decreased while the distribution of N_{eff} was broadened in both grains and boundaries.

where ΔS_R is the PSD of R_s . From $N_{\text{eff}} \sim (\Delta S_I/I^2) = (\Delta S_R/R_s^2)$, the relation $N_{\text{eff}} \sim (R_s)^w$ is obtained, which explains the correlation between N_{eff} and R_s . In our result, the exponent w was approximately 0.4, which is similar to that observed in an FET channel including the grain boundary in monolayer MoS₂⁴⁰. This kind of scaling behavior has been observed in many percolation systems where the exponents varied according to the material, geometry and temperature^{38–41}. On the other hand, the unique negative correlation for the grain regions can be explained by the electrical transport mechanism in monolayer MoS₂. It was suggested that the charge transport in few-layered MoS₂ is dominated by hopping through localized states, which originates from sulfur vacancies^{14,30,42}. At room temperature (~ 300 K), the dominating transport mechanism in MoS₂ should be nearest-neighbor hopping³⁰. In this mechanism, the conductivity (σ) is expressed as $\sigma \sim \exp(-1/a^2kTN_{\text{eff}})$, where ' a ' is an average defect distance and N_{eff} is the density of states near the Fermi level, which corresponds to N_{eff} ³⁰. The equation indicates that if there are many sulfur vacancies in a region (high N_{eff}), the hopping probability for the carriers will be high due to the high density of vacancy-induced hopping sites, resulting in a high conductivity. In the plot, the data points for the grain regions are fitted well by the equation $R_s \sim \exp(1/a^2kTN_{\text{eff}})$. As a fitting parameter, the average defect distance (a) was estimated to be ~ 1.97 nm, which was very close to the reported value of ~ 1.7 nm³⁰. Previous observations based on transmission electron microscopy (TEM) revealed that sulfur vacancies are the most common defects in monolayer MoS₂^{30,36}. Additionally, it should be mentioned that the reported density of trap states from sulfur vacancies was comparable to our N_{eff} value³⁰. Therefore, the negative correlation between N_{eff} and R_s for the grain regions could be attributed to the sulfur vacancies playing a key role for both charge transport and charge trap generation in monolayer MoS₂.

Enhancement of photoconductivity by localized charge traps. To investigate the effect of charge traps on photoconductive charge transport in monolayer MoS₂, we measured the MoS₂ film under dark and illuminated conditions. Figure 4(a) shows a current map (I_{dark}) of the MoS₂ monolayer measured under the dark condition. A DC bias voltage of 5 V was applied to the Au/Ti electrode. In the map, many grains were observed since we scanned an area ($10 \times 10 \mu\text{m}^2$) larger than that of individual grains. The grains and boundaries were distinguished by relatively high and low current values, respectively.

Figure 4(b) is the map of the current changes (ΔI) caused by light illumination. We used a white light source (LS-F100HS, Light Bank) with an intensity of ~ 100 mW/cm². Here, a current map was first measured under the dark condition, with the measurement repeated under illumination. After illumination, the currents in the grains were found to increase by more than 10^{-5} A, resulting in ~ 7.5 times higher current values than before illumination. On the other hand, the currents in the boundaries increased by only a factor of ~ 4 , indicating rather small changes (10^{-6} – 10^{-5} A). The current increase was caused by photocarrier generation in the MoS₂ layer^{9,43}.

Previously, defects such as charge traps in MoS₂ were reported to assist the recombination of photogenerated carriers as recombination centers, and, thus, to reduce the photocurrents⁴³, which explains the low photocurrent in boundaries. It is also notable that there were clear differences in current values between individual grains. The current differences between individual grains were as large as 30% of the average current value of all the grains. This inter-grain current difference can be attributed to an energy band modulation that presumably arises from the random crystal orientation and strain of MoS₂ grains grown via the CVD method^{24,34}.

Figure 4(c) shows a map of the charge trap density when the MoS₂ film was under the dark condition ($N_{\text{eff, dark}}$). The $N_{\text{eff, dark}}$ map was calculated using the current map (Fig. 4(a)) and the noise PSD map at 17.3 Hz. The $N_{\text{eff, dark}}$ values were on the order $\sim 10^{14} \text{ cm}^{-2} \text{ eV}^{-1}$ and found to be higher in boundaries than in grains. This result is consistent with that shown in Fig. 3(e). The difference in $N_{\text{eff, dark}}$ between individual grains could arise from the grain-growing process, as mentioned in Fig. 4(b).

Figure 4(d) shows a map of the charge trap density changes (ΔN_{eff}) in the MoS₂ film due to illumination. The map was obtained by subtracting the $N_{\text{eff, dark}}$ map (Fig. 4(c)) from a N_{eff} map measured under light illumination. The ΔN_{eff} map shows a considerable increase in the number of charge traps. The average values for ΔN_{eff} were $\sim 2.85 \times 10^{14} \text{ cm}^{-2} \text{ eV}^{-1}$ in grains and $\sim 7.03 \times 10^{14} \text{ cm}^{-2} \text{ eV}^{-1}$ in boundaries. This result was in accordance with previous studies showing that light irradiation can increase the charge traps in MoS₂ layers by various mechanisms such as bond breaking, removal of atoms^{44,45}. On the other hand, O₂ or water molecules physisorbed onto MoS₂ surfaces can work as a charge traps. Such physisorbed molecules could be removed by light illumination, reducing the charge trap density N_{eff} . The large increase in charge trap density in our experiments indicates that charge trap generation by light illumination overwhelmed the effect of the desorption of such physisorbed molecular species.

Figure 4(e) shows a scatter plot showing the relation between the charge trap density under the dark condition $N_{\text{eff, dark}}$ and photocurrent level ΔI in the grains and boundaries of the MoS₂ film. Each data point in the plot represents $N_{\text{eff, dark}}$ and ΔI values for the pixel area shown in Fig. 4b,c. In the plot, the data points for the boundary regions show no special correlation. However, a positive correlation between $N_{\text{eff, dark}}$ and ΔI is observed in the grain regions, as indicated by the yellow fitted line with a slope of ~ 0.9 . Considering that traps were previously reported to act as recombination centers, resulting in a decreased photocurrent⁴⁶, this result is quite unusual. One possible explanation for this anomalous enhancement of the photocurrent by charge traps is that the photocurrent in few-layer MoS₂ is significantly affected by O₂ molecules on the MoS₂ surface^{43,47}. Previous studies showed that both dark current and photocurrent levels for monolayer MoS₂ were much lower in ambient air than in vacuum, attributing the difference to chemisorbed O₂ molecules, which captured a large portion of the electrons from MoS₂^{43,47}. When the MoS₂ was illuminated with light under ambient conditions, electron-hole pairs were generated by photoexcitation. Then, the photogenerated holes recombined with the electrons captured by some chemisorbed O₂ molecules, and the discharged O₂ molecules were desorbed from the surface^{43,47}. In this case, the photogenerated electrons, which might be captured by the chemisorbed O₂ molecules, were now free and acted as a charge carrier. Thus, the number of free electrons in the MoS₂ channel increased, and the current increase (ΔI) should be proportional to the number of desorbed O₂ molecules generated by illumination. On the other hand, before illumination, the O₂ molecules were chemisorbed on sulfur vacancies⁹ which were responsible for $N_{\text{eff, dark}}$. In this case, the MoS₂ regions with *more sulfur vacancies (or larger $N_{\text{eff, dark}}$)* should have *more chemisorbed O₂ molecules* before illumination^{30,36}, and, following light illumination, they should also have a *larger number of desorbed O₂ molecules* and a *larger current increase*. Therefore, the proportional relationships lead to the proportionality between ΔI and $N_{\text{eff, dark}}$, explaining the fitted line with a slope close to 1 in the log-log plot. Our result revealed the anomalous enhancement of the photocurrent due to noise sources such as charge traps, which can be important in applications of MoS₂ to optoelectronics since electrical noise is often a key parameter determining device performance.

Figure 4(f) shows a scatter plot showing the distributions of the N_{eff} and R_s values for the monolayer MoS₂ under dark and illuminated conditions. Each data point represents the N_{eff} and R_s values of each pixel area in the maps. There are two groups of data points obtained under dark (high R_s) and illuminated (low R_s) conditions. Each group consists of the data points from grains and boundaries, which were distinguished using R_s maps (Fig. S2 in the Supplementary Information). The distribution of data points obtained under the dark condition was similar to that shown in Fig. 3(f), exhibiting different $N_{\text{eff}}-R_s$ correlations between grains and boundaries. On the other hand, under illumination, R_s was generally decreased while the distribution of N_{eff} was broadened in both grain and boundary regions. The broadening of the N_{eff} distribution was the result of a large increase in N_{eff} in most regions and a decrease in N_{eff} in only a few regions. The increase in N_{eff} was mainly caused by defect generation due to absorbed photon energy^{44,45}. Additionally, localized states filled with charges under the dark condition could trap charge carriers after photoexcitation of the occupied charges, contributing to the increase in N_{eff} . On the other hand, the desorption of physically adsorbed O₂ molecules from the MoS₂ surface could decrease N_{eff} . It is also worth mentioning that the N_{eff} distribution is rather broadened by the light illumination, resulting in weakened $N_{\text{eff}}-R_s$ correlation. Presumably, under dark conditions, most of the charge traps are sulfur vacancies contributing to charge conduction as a hopping site³⁰. However, light illumination generated various charge traps, which may not work as a hopping site, such as Mo vacancies and large atomic holes⁴⁴.

Conclusions

In conclusion, we successfully imaged how localized charge traps enhanced the photoconductivity in the grain structures of monolayer MoS₂. By laterally scanning a conducting AFM probe used to make direct contact with a monolayer MoS₂ sample, electrical currents and noise transmitted through the probe were simultaneously mapped. The mapping data were analyzed to obtain the distribution maps for the sheet resistance and charge trap density in the grain structures of MoS₂. The result showed that both the sheet resistance and charge trap density were higher in the grain boundaries than in the grains. We found a unique negative correlation between

the charge trap density and sheet resistance, which was attributed to the role of sulfur vacancies acting as both hopping sites and charge traps in monolayer MoS₂. Furthermore, the photocurrent exhibited a positive scaling relation with the charge trap density since photogenerated holes recombined with electrons captured by oxygen molecules absorbed on sulfur vacancies. Since our strategy enabled us to map the nanoscale effect of localized charge traps on the photoconductive carrier transport, it should be a versatile tool that can be used for basic noise studies and applications based on versatile two-dimensional materials.

Methods

Monolayer MoS₂ synthesis. Large-area monolayer MoS₂ films were grown by a dual-heating zone chemical vapor deposition (CVD) system. The molybdenum trioxide (MoO₃) powder and a carefully cleaned SiO₂ substrate were heated inside a furnace up to ~750 °C, with the sulfur (S) powder heated inside an electric heater up to ~200 °C. The pressure inside a quartz tube was maintained at ~10 Torr with Ar carrying gas.

Au/Ti contact electrode deposition. The CVD-grown MoS₂ film was covered by a shadow mask used for electrode patterning without any surface treatments. To fabricate the electrodes, Ti (10 nm) and Au (100 nm) were deposited with a deposition rate of 0.5 Å/s at a pressure of ~10⁻⁶ Torr in an electron beam evaporator system.

Raman spectroscopy. Raman spectra were measured for the CVD-grown MoS₂ to characterize the thickness. The measurements were performed with a Raman spectroscopy system (XperRam 200, Nanobase) using a 532 nm laser.

References

- Radisavljevic, B., Radenovic, A., Brivio, J., Giacometti, V. & Kis, A. Single-layer MoS₂ transistors. *Nat. Nanotechnol.* **6**, 147–150 (2011).
- Mak, K. F., Lee, C., Hone, J., Shan, J. & Heinz, T. F. Atomically thin MoS₂: a new direct-gap semiconductor. *Phys. Rev. Lett.* **105**, 136805 (2010).
- Wang, Q. H., Kalantar-Zadeh, K., Kis, A., Coleman, J. N. & Strano, M. S. Electronics and optoelectronics of two-dimensional transition metal dichalcogenides. *Nat. Nanotechnol.* **7**, 699–712 (2012).
- Jariwala, D., Sangwan, V. K., Lauhon, L. J., Marks, T. J. & Hersam, M. C. Emerging device applications for semiconducting two-dimensional transition metal dichalcogenides. *ACS Nano* **8**, 1102–1120 (2014).
- Lopez-Sanchez, O., Lembke, D., Kayci, M., Radenovic, A. & Kis, A. Ultrasensitive photodetectors based on monolayer MoS₂. *Nat. Nanotechnol.* **8**, 497–501 (2013).
- Yin, Z. *et al.* Preparation of MoS₂-MoO₃ hybrid nanomaterials for light-emitting diodes. *Angew. Chem. Int. Ed.* **53**, 12560–12565 (2014).
- Tsai, M.-L. *et al.* Monolayer MoS₂ heterojunction solar cells. *ACS Nano* **8**, 8317–8322 (2014).
- Hooge, F. N., Kleinpenning, T. G. M. & Vandamme, L. K. J. Experimental studies on 1/f noise. *Rep. Prog. Phys.* **44**, 479–532 (1981).
- Nan, H. *et al.* Strong photoluminescence enhancement of MoS₂ through defect engineering and oxygen bonding. *ACS Nano* **8**, 5738–5745 (2014).
- Xie, J. *et al.* Defect-rich MoS₂ ultrathin nanosheets with additional active edge sites for enhanced electrocatalytic hydrogen evolution. *Adv. Mater.* **25**, 5807–5813 (2013).
- Sangwan, V. K. *et al.* Low-frequency electronic noise in single-layer MoS₂ transistors. *Nano Lett.* **13**, 4351–4355 (2013).
- Renteria, J. *et al.* Low-frequency 1/f noise in MoS₂ transistors: relative contributions of the channel and contacts. *Appl. Phys. Lett.* **104**, 153104 (2014).
- Sharma, D. *et al.* Electrical transport and low-frequency noise in chemical vapor deposited single-layer MoS₂ devices. *Nanotechnology* **25**, 155702 (2014).
- Ghatak, S., Mukherjee, S., Jain, M., Sarma, D. D. & Ghosh, A. Microscopic origin of low frequency noise in MoS₂ field-effect transistors. *APL Mater.* **2**, 092515 (2014).
- Lee, H. *et al.* Nanoscale direct mapping of noise source activities on graphene domains. *ACS Nano* **10**, 10135–10142 (2016).
- Shekhar, S., Cho, D., Lee, H., Cho, D.-G. & Hong, S. Nanoscale direct mapping of localized and induced noise sources on conducting polymer films. *Nanoscale* **8**, 835–842 (2016).
- Cho, D. *et al.* Direct mapping of electrical noise sources in molecular wire-based devices. *Sci. Rep.* **7**, 43411 (2017).
- Park, W. *et al.* Photoelectron spectroscopic imaging and device applications of large-area patternable single-layer MoS₂ synthesized by chemical vapor deposition. *ACS Nano* **8**, 4961–4968 (2014).
- Lee, C. *et al.* Anomalous lattice vibrations of single- and few-layer MoS₂. *ACS Nano* **4**, 2695–2700 (2010).
- Yoon, H. S. *et al.* Layer dependence and gas molecule absorption property in MoS₂ schottky diode with asymmetric metal contacts. *Sci. Rep.* **5**, 10440 (2015).
- Sangwan, V. K. *et al.* Multi-terminal memtransistors from polycrystalline monolayer molybdenum disulfide. *Nature* **554**, 500 (2018).
- Hung, K. K., Ko, P. K., Hu, C. & Cheng, Y. C. A unified model for the flicker noise in metal-oxide-semiconductor field-effect transistors. *IEEE Trans. Electron Devices* **37**, 654–665 (1990).
- Magnone, P. *et al.* 1/f noise in drain and gate current of MOSFETs with high-*k* gate stacks. *IEEE Trans. Device Mater. Reliab.* **9**, 180–189 (2009).
- Liu, Z. *et al.* Strain and structure heterogeneity in MoS₂ atomic layers grown by chemical vapour deposition. *Nat. Commun.* **5**, 5246 (2014).
- Najmaei, S. *et al.* Vapour phase growth and grain boundary structure of molybdenum disulphide atomic layers. *Nat. Mater.* **12**, 754–759 (2013).
- Ly, T. H. *et al.* Misorientation-angle-dependent electrical transport across molybdenum disulfide grain boundaries. *Nat. Commun.* **7**, 10426 (2016).
- Huang, Y. L. *et al.* Bandgap tunability at single-layer molybdenum disulphide grain boundaries. *Nat. Commun.* **6**, 6298 (2015).
- Zhou, W. *et al.* Intrinsic structural defects in monolayer molybdenum disulfide. *Nano Lett.* **13**, 2615–2622 (2013).
- Precner, M. *et al.* Evolution of metastable defects and its effect on the electronic properties of MoS₂ films. *Sci. Rep.* **8**, 6724 (2018).
- Qiu, H. *et al.* Hopping transport through defect-induced localized states in molybdenum disulphide. *Nat. Commun.* **4**, 2642 (2013).
- Bertolazzi, S. *et al.* Engineering chemically active defects in monolayer MoS₂ transistors via ion-beam irradiation and their healing via vapor deposition of alkanethiols. *Adv. Mater.* **29**, 1606760 (2017).
- Yu, Z. *et al.* Towards intrinsic charge transport in monolayer molybdenum disulfide by defect and interface engineering. *Nat. Commun.* **5**, 5290 (2014).
- Schmidt, H. *et al.* Transport properties of monolayer MoS₂ grown by chemical vapor deposition. *Nano Lett.* **14**, 1909–1913 (2014).
- van der Zande, A. M. *et al.* Grains and grain boundaries in highly crystalline monolayer molybdenum disulphide. *Nat. Mater.* **12**, 554–561 (2013).

35. Jayaraman, R. & Sodini, C. G. A $1/f$ noise technique to extract the oxide trap density near the conduction-band edge of silicon. *IEEE Trans. Electron Devices* **36**, 1773–1782 (1989).
36. Hong, J. *et al.* Exploring atomic defects in molybdenum disulphide monolayers. *Nat. Commun.* **6**, 6293 (2015).
37. Na, J. *et al.* Low-frequency noise in multilayer MoS₂ field-effect transistors: the effect of high- k passivation. *Nanoscale* **6**, 433–441 (2014).
38. Kim, T.-Y. *et al.* Analysis of the interface characteristics of CVD-grown monolayer MoS₂ by noise measurements. *Nanotechnology* **28**, 145702 (2013).
39. Pennetta, C., Trefan, G. & Reggiani, L. Scaling law of resistance fluctuations in stationary random resistor networks. *Phys. Rev. Lett.* **85**, 5238–5241 (2000).
40. Kim, J.-K. *et al.* Analysis of noise generation and electric conduction at grain boundaries in CVD-grown MoS₂ field effect transistors. *Nanotechnology* **28**, 47LT01 (2017).
41. Lee, S. B. *et al.* Large $1/f$ noise of unipolar resistance switching and its percolating nature. *Appl. Phys. Lett.* **95**, 122112 (2009).
42. Cho, K. *et al.* Electrical and optical characterization of MoS₂ with sulfur vacancy passivation by treatment with alkanethiol molecules. *ACS Nano* **9**, 8044–8053 (2015).
43. Zhang, W. *et al.* High-gain phototransistors based on a CVD MoS₂ monolayer. *Adv. Mater.* **25**, 3456–3461 (2013).
44. Paradisanos, I., Kymakis, E., Fotakis, C., Kioseoglou, G. & Stratakis, E. Intense femtosecond photoexcitation of bulk and monolayer MoS₂. *Appl. Phys. Lett.* **105**, 041108 (2014).
45. Castellanos-Gomez, A. *et al.* Laser-thinning of MoS₂: on demand generation of a single-layer semiconductor. *Nano Lett.* **12**, 3187–3192 (2012).
46. Wang, H., Zhang, C. & Rana, F. Ultrafast dynamics of defect-assisted electron-hole recombination in monolayer MoS₂. *Nano Lett.* **15**, 339–345 (2014).
47. Lee, Y. *et al.* Trap-induced photoresponse of solution-synthesized MoS₂. *Nanoscale* **8**, 9193–9200 (2016).

Acknowledgements

This work was supported by BioNano Health-Guard Research Center funded by the Ministry of Science, ICT and Future Planning (MSIP) of Korea as Global Frontier Project (No. H-GUARD_2013M3A6B2078961). T.-Y.K. and T.L. acknowledge the financial support of the National Creative Research Laboratory program (No. 2012026372) from the National Research Foundation of Korea (NRF) grant. S.H. also acknowledges the support from the National Research Foundation of Korea (NRF) grants (Nos 2017R1A2B2006808, 2014M3A7B4051591).

Author Contributions

M.Y. performed the experiments, analyzed the data, and wrote the manuscript. T.-Y.K. and T.L. provided the MoS₂ sample and Raman spectroscopy data. S.H. planned and supervised the project. All authors reviewed the manuscript.

Additional Information

Supplementary information accompanies this paper at <https://doi.org/10.1038/s41598-018-34209-w>.

Competing Interests: The authors declare no competing interests.

Publisher's note: Springer Nature remains neutral with regard to jurisdictional claims in published maps and institutional affiliations.



Open Access This article is licensed under a Creative Commons Attribution 4.0 International License, which permits use, sharing, adaptation, distribution and reproduction in any medium or format, as long as you give appropriate credit to the original author(s) and the source, provide a link to the Creative Commons license, and indicate if changes were made. The images or other third party material in this article are included in the article's Creative Commons license, unless indicated otherwise in a credit line to the material. If material is not included in the article's Creative Commons license and your intended use is not permitted by statutory regulation or exceeds the permitted use, you will need to obtain permission directly from the copyright holder. To view a copy of this license, visit <http://creativecommons.org/licenses/by/4.0/>.

© The Author(s) 2018